AIAA JOURNAL
Vol. 45, No. 12, December 2007

Nonpremixed Combustion in an Accelerating Transonic Flow Undergoing Transition

Felix Cheng,* Feng Liu,† and William A. Sirignano‡
University of California, Irvine, Irvine, California 92697-3975

DOI: 10.2514/1.31146

Mixing layers composed of fuel and oxidizer streams passing through straight channels are studied by performing two-dimensional numerical simulations. Both nonaccelerating and accelerating mixing layers are studied. In the nonaccelerating cases, the flow remains at low subsonic speed throughout the channel. In the accelerating cases, the flow accelerates from low subsonic speed to low supersonic speed through the channel. In this paper, we focus on the development of the mixing layers from laminar flow to the transition regime. The full Navier–Stokes equations coupled with multiple-species equations and the energy equations with chemical reactions are solved using a finite difference numerical scheme. Both forced and unforced instabilities are considered, but the use of forced disturbances is found to be not essential to this study. The reacting mixing layers with or without acceleration are more unstable than the corresponding nonreacting mixing layers in terms of the fluctuations of kinetic energy. For the reacting cases, both positive and negative vortices are produced. The positive vorticity is generated by the baroclinic effect associated with the large density gradient and is more pronounced in the reacting and accelerating case, in which a large pressure gradient exists. The accelerating mixing layers show stabilizing effects, and the overall chemical conversion rate reduces due to the acceleration.

I. Introduction

DESIGNERS of jet engines are attempting to increase the thrust-to-weight ratio and to widen the range of engine operation. Because the flow in a turbine passage is accelerating and power is extracted from the flow, it is possible to add heat without raising the flow temperature beyond the turbine-blade material limit. Sirignano and Liu [1,2] showed by thermodynamic analysis that the thrust of aircraft turbojet and turbofan engines can be increased significantly with little increase in fuel consumption by intentionally burning fuel in the turbine stages. For ground-based gas turbines, benefits have been shown to occur in the power-to-weight ratio and efficiencies [1]. An exothermic chemical reaction in the accelerating flow through a turbine passage therefore offers an opportunity for a major technological improvement. In addition to improving thrust or efficiency, this technology also shows promise in reduced pollutants formation due to the reduction of peak temperature in the combustion process of the accelerating flow.

The geometry of the turbine passage is rather complex. To simplify the problem while retaining the major physics in the present study, we create a model problem in this paper in which a mixing layer of fuel and oxidizer streams going through a channel with imposed streamwise pressure gradients is studied. We are not performing numerical simulations on the actual flows in a turbine passage; instead, we focus on the fundamental physics such as the effects of streamwise acceleration on the instability and the chemical reactions in the reacting and accelerating mixing layers.

There has been little previous research on steady-state multidimensional flows with mixing and chemical reactions in the presence of strong pressure gradients. Research has been done on high-speed nonaccelerating and reacting flows. A comprehensive literature review was done by Sirignano and Kim [3]. In that paper, they also obtained similarity solutions for laminar two-dimensional reacting and nonreacting mixing layers with a favorable pressure gradient in the primary flow direction. Fang et al. [4] extended that study to mixing layers with arbitrary pressure gradients by using a finite difference method for the boundary-layer equations. The influence of pressure gradients, initial temperature, initial pressure, initial velocity, and transport properties were studied. Mehring et al. [5] performed a numerical study on a reacting turbulent accelerating mixing layer based on the laminar boundary-layer calculations by Fang et al. [4]. Cai et al. [6] developed a finite volume method for solving the two-dimensional compressible Favre-averaged Navier–Stokes equations with chemical reactions using the Baldwin–Lomax turbulence model.

Although the steady-state calculations provide important insight into the fundamental physics of multidimensional mixing layers with chemical reactions and strong pressure gradients, they are unable to describe the mechanism by which the flows evolve being from laminar to turbulent. Motivated by this, our primary objective of this paper is to investigate the instability of two-dimensional reacting and accelerating shear layers from the linear stage to the early transitional stage and its effects on the combustion process. As a result, the understanding of the instability of nonreacting and nonaccelerating shear layers serves as a foundation of our research.

The instability of nonreacting and nonaccelerating mixing layers has been studied extensively by experiments, stability theory, and numerical simulations. A comprehensive overview of those works can be found in Ho and Huerre [7]. Studies of the development of vortical structures in unstable mixing layers are of particular interest to our research. The roll-up of the vortex sheet and the pairing and merging of the vortices have tremendous influence on the mixing of two fluids, the growth of the boundary layers, and hence the combustion process. An early theoretical work was done by Michalke [8] in an attempt to study the formation of vortices in free boundary layers by means of stability theory using a hyperbolic-tangent velocity profile. By examining the vorticity distribution of the perturbed flow, they found a tendency of roll-up of the vortex layer. Roll-up of a laminar boundary layer and pairing of vortices were also observed by Freymuth [9] in experiments.

The interaction of two-dimensional vortices in a mixing layer was studied by Winant and Browand [10] experimentally. Pairings of

Presented as Paper 1417 at the 43rd AIAA Aerospace Sciences Meeting and Exhibit, Reno NV, 10–13 January 2005; received 20 March 2007; revision received 8 August 2007; accepted for publication 9 August 2007.

*Graduate Student Researcher, Department of Mechanical and Aerospace Engineering. Member AIAA.
†Professor, Department of Mechanical and Aerospace Engineering. Associate Fellow AIAA.
‡Professor, Department of Mechanical and Aerospace Engineering. Fellow AIAA.

discrete vortices were observed, and they occurred continuously throughout the channel. It was also found that the momentum thickness had a linear growth with downstream distance in the region where pairing of vortices occurred repeatedly. The merging of vortices in unforced mixing layers appears in an unpredictable fashion, because the flows are excited by random noises. However, one can manipulate the merging process by applying external forcing. Ho and Huang [11], by perturbing the mixing layer with subharmonic frequencies, managed to control the number of vortices that merge simultaneously. Moreover, the locations of merging became localized. Davis and Moore [12] performed a numerical study on vortex merging in mixing layers and found consistent results with Ho and Huang [11]. They were able to predict and control the merging patterns of the discrete vortices. Numerical simulations of three-dimensional temporally evolving plane mixing layers were performed by Moser and Rogers [13,14]. Infinitesimal three-dimensional disturbances were imposed initially. Spanwise vorticity rolled up into corrugated spanwise rollers, and predominantly streamwise rib vortices developed in the braid region between the spanwise rollers. The development of three-dimensionality, the nonlinear evolution of three-dimensional disturbances with spanwise vortices during pairings, and the transition mechanisms were studied in detail. Although the development of three-dimensional structures are absent in our two-dimensional study, we focus on the early stages of transition in which the development of the mixing layer is dominated by a 2-D mechanism. So our 2-D simulations will be able to capture the important physics.

In reacting mixing layers, the stability characteristics could be different from those in nonreacting mixing layers due to the modifications of the flow profiles caused by the chemical reactions. The effects of heat release on the instability of reacting mixing layers were studied by Shin and Ferziger [15] by linear stability theory. An inviscid low-Mach-number stability equation was derived and solved numerically. With a sufficient amount of heat release, multiple unstable modes (referred to as the outer modes) in addition to the central mode (the unstable mode associated with the central inflection point of the mean-velocity profile) were found. The outer modes arose due to the modifications of the density and velocity profiles caused by the chemical reactions and were quite insensitive to the further increases in heat release. The central modes were suppressed significantly by the further increases in heat release so that the outer modes could become the dominant unstable modes. Shin and Ferziger [16] extended their previous work to include effects of high Mach numbers. Multiple supersonic unstable modes were found in both the nonreacting and reacting flows when the phase velocity of the disturbance was supersonic relative to the freestream. The supersonic modes became less unstable with increasing Mach number but more unstable with increasing heat release. These modes seemed not to enhance mixing of the two streams.

Direct numerical simulations (DNS) of reacting mixing layers show general agreements with linear stability analysis. McMurtry et al. [17] performed direct numerical simulations of a low-Mach-number two-dimensional mixing layer undergoing a single-step exothermic chemical reaction. The results showed that the rate of chemical products formed, the thickness of the mixing layer, and the entrainment of mass into the layer all decreased with increasing rate of heat release. In another three-dimensional DNS study by McMurtry et al. [18], reduction in the entrainment of the reactants and the global reaction rate was again observed. They found that the baroclinic torque and thermal expansion in the mixing layer produced changes in the flame vortex structures that caused more diffuse vortices than in the constant-density nonreacting case. The rotation rates of the large-scale structures were lowered, resulting in reduced growth rate and entrainment of the unmixed fluids. Soteriou and Ghoniem [19] also performed a two-dimensional numerical simulation on the vortex dynamics of a low-Mach-number, forced spatially developing, high-Reynolds-number, reacting shear layer. Overall reduction of the cross-stream growth of the mixing region was found, and the entrainment of fluids and vortex merging were also inhibited.

Hermanson and Dimotakis [20] also found consistent results with linear stability theory and DNS by conducting experiments to examine the effects of heat release in a planar reacting mixing layer formed between two streams. The adiabatic temperature in the experiments corresponded to moderate heat release. Their results showed that the growth rate of the layer decreased slightly with increasing heat release, and the overall entrainment of mass into the layer was substantially reduced. They also found that the mean structure spacing decreased with increasing temperature and suggested that the vortex amalgamation was inhibited.

In the present paper, mixing layers composed of fuel and oxidizer streams in straight channels are studied by performing numerical simulations. The main objective is to study the accelerating and chemically reacting mixing layers undergoing transition. The discussions of the governing equations and numerical scheme are presented in Sec. II. The boundary conditions are given in Sec. III. The unforced nonaccelerating cases are presented in Sec. IV.A, and the effects of forcing on the nonaccelerating cases are discussed in Sec. IV.B. The unforced mixing layers with streamwise acceleration are presented in Sec. IV.C, and the forced accelerating mixing layers are presented in Sec. IV.D. The concluding remarks are given in Sec. V.

II. Governing Equations and the Numerical Method

The flow within a turbine-blade row is at high speed and often transonic. There are large streamwise and transverse gradients of pressure, density, and velocity in the flowfield. Because the geometry of the turbine passage is rather complex, we simplify the physical model to a straight converging–diverging channel in this paper. For this simplified geometry, the physics associated with the streamwise acceleration is retained but the effects of transverse acceleration are absent. The study of a curved converging–diverging channel in which strong streamwise and transverse pressure gradients exist is underway; however, it is beyond the scope of this paper. Because we only consider flows evolving from laminar stage to transitional stage, small-scale turbulent structures are not resolved in this paper. Also, at the early stage of transition, the development of the mixing layer is dominated by large-scale two-dimensional vortices [10]. The two-dimensional simulations are able to capture the important physics of the mixing layer in its early stage of transition while maintaining relatively low computational cost. The effects of three-dimensionality will be neglected as an approximation.

The geometry of the computational domain and the flow configuration are shown in Fig. 1. The mixing layer enters the channel from the left through the inlet plane. The upper stream is air

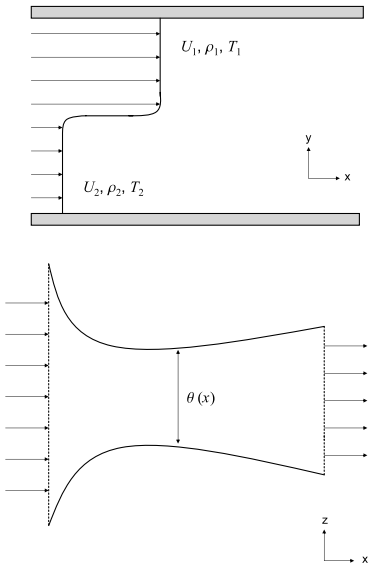

Fig. 1 Top and side views of the converging–diverging channel; subscript 1 denotes air and subscript 2 denotes fuel.

and the lower stream is methane in all cases. The channel width in the z direction is given as θ. Because the flow is two-dimensional, there is no variation of flow properties in the z direction, and θ only serves to impose streamwise pressure gradients to the flowfield; θ varies in the x direction only and it is designed in such a way that the mixing layer will be choked for the given inlet conditions and back pressure. For the nonaccelerating cases, θ is constant throughout the channel.

The governing equations, with the channel width incorporated, are the two-dimensional, compressible, multicomponent, modified Navier–Stokes equations with chemical source terms. There are a total of eight governing equations. They are the continuity equation for the total mass density, the momentum equations in the x and y directions, the energy equation, and the continuity equations for the individual mass densities of O_2, CH_4, H_2O, and CO_2. Perfect gas is assumed. The equations written in conservation form are as follows:

$$\frac{\partial \theta \mathbf{w}}{\partial t} + \frac{\partial \theta \mathbf{f}}{\partial x} + \frac{\partial \theta \mathbf{g}}{\partial y} - \frac{\partial \theta \mathbf{f}_\mu}{\partial x} - \frac{\partial \theta \mathbf{g}_\mu}{\partial y} = \theta \mathbf{s} \tag{1}$$

where $\mathbf{w}$ is the vector of the conservative variables of mass, momentum, and energy; the vectors $\mathbf{f}$ and $\mathbf{g}$ are the inviscid fluxes; $\mathbf{f}_\mu$ and $\mathbf{g}_\mu$ the viscous fluxes; and $\mathbf{s}$ is the source term. These terms are given as

$$\mathbf{w} = \begin{pmatrix} \rho \\ \rho u \\ \rho v \\ \rho E \\ \rho_n \end{pmatrix}, \qquad \mathbf{s} = \begin{pmatrix} 0 \\ \frac{p}{\theta}\frac{\partial \theta}{\partial x} \\ \frac{p}{\theta}\frac{\partial \theta}{\partial y} \\ \dot{Q} \\ \dot{\omega}_n \end{pmatrix} \tag{2}$$

$$\mathbf{f} = \begin{pmatrix} \rho u \\ \rho u u + p \\ \rho v u \\ \rho H u \\ \rho_n u \end{pmatrix}, \qquad \mathbf{g} = \begin{pmatrix} \rho v \\ \rho u v \\ \rho v v + p \\ \rho H v \\ \rho_n v \end{pmatrix} \tag{3}$$

$$\mathbf{f}_\mu = \begin{pmatrix} 0 \\ \tau_{xx} \\ \tau_{yx} \\ u\tau_{xx} + v\tau_{yx} - q_x - \sum_{n=1}^{N} \rho_n u_{dn} h_n \\ -\rho_n u_{dn} \end{pmatrix} \tag{4}$$

$$\mathbf{g}_\mu = \begin{pmatrix} 0 \\ \tau_{xy} \\ \tau_{yy} \\ u\tau_{xy} + v\tau_{yy} - q_y - \sum_{n=1}^{N} \rho_n v_{dn} h_n \\ -\rho_n v_{dn} \end{pmatrix} \tag{5}$$

In the preceding equations, t is time; ρ_n is the density for species n, where $1 \le n \le N$, and N is the total number of species; p is the pressure; μ is the molecular viscosity; and u and v are the flow velocity components in the x and y directions, respectively. Other quantities are defined in the following equations:

$$\tau_{ij} = 2\mu\left[\frac{1}{2}\left(\frac{\partial u_i}{\partial x_j} + \frac{\partial u_j}{\partial x_i}\right) - \frac{1}{3}\frac{\partial u_k}{\partial x_k}\delta_{ij}\right] \tag{6}$$

$$q_j = -C_p \frac{\mu}{Pr}\frac{\partial T}{\partial x_j} \tag{7}$$

$$h = \sum_{n=1}^{N} Y_n h_n, \qquad h_n = \int_{T_0}^{T} C_{pn}\, \mathrm{d}T \tag{8}$$

$$H = h + \tfrac{1}{2}(u^2 + v^2) \tag{9}$$

$$E = H - \frac{p}{\rho} \tag{10}$$

$$\dot{Q} = -\sum_{n=1}^{N} \dot{\omega}_n h_n^0 \tag{11}$$

$$\rho_n \mathbf{V}_{dn} = -\rho D_n \nabla\left(\frac{\rho_n}{\rho}\right) = -\rho D_n \nabla Y_n \tag{12}$$

where τ_{ij} is the shear stress tensor (the standard tensor notation is used: the subscript indices i and j take either value 1 or 2 to represent the x and y components, respectively; h_n^0 is the heat of formation of species n at the reference temperature T_0; C_{pn} is the specific heat at constant pressure of species n,; $\mathbf{V}_{dn} = (u_{dn}, v_{dn})$ is the diffusion velocity of species n; and D_n is the diffusion coefficient. Because we assume unity Schmidt number and Prandtl number, $D_n = \mu/\rho$ for all species. C_{pn} and h_n vary with temperature; they are given by the NASA polynomials.

Methane (CH_4) is used for the current computations, although the method is not restricted to only one type of fuel. The combustion process is described by a one-step overall chemical reaction as follows:

$$C\,H_4 + 2O_2 + 7.52N_2 \rightarrow CO_2 + 2H_2O + 7.52N_2$$

The chemical kinetics rate for the fuel is

$$\dot{\omega}_F = -W_F A e^{-E_a/RT}[\text{fuel}]^a[O_2]^b \tag{13}$$

where the brackets [ ] represent molar concentration in mol/cm^3, W_F is the molecular weight of fuel. For methane (CH_4), the parameter values [21] are $A = 2.8 \times 10^9$ 1/s, $E_a = 48.4$ kcal/mol, $a = -0.3$, and $b = 1.3$.

In the solution procedure, the average gas constant R, molecular weight W, and viscosity coefficient μ can be obtained by the following equations:

$$R = \sum_{n=1}^{N} R_n Y_n \tag{14}$$

$$\frac{1}{W} = \sum_{n=1}^{N} \frac{1}{W_n} Y_n \tag{15}$$

$$\mu = \sum_{n=1}^{N} \mu_n(T) Y_n \tag{16}$$

The molecular viscosity coefficient of each species μ_n is obtained [22] by using the Sutherland law:

$$\frac{\mu_n}{\mu_{0n}} = \left(\frac{T}{T_0}\right)^{\frac{3}{2}} \frac{T_0 + 110}{T + 110} \tag{17}$$

where T_0 is the reference temperature (298.15 K), and μ_{0n} is the reference viscosity evaluated at T_0.

Before discretization, Eq. (1) in the physical domain is transformed to a uniform computational domain by the following transformation relations:

$$\xi = \xi(x, y) \Leftrightarrow x = x(\xi, \eta) \tag{18}$$

$$\eta = \eta(x, y) \Leftrightarrow y = y(\xi, \eta) \tag{19}$$

The transformed governing equation in the computational domain is written as follows:

$$\frac{\partial(\theta\hat{\mathbf{w}})}{\partial t} + \frac{\partial(\theta\hat{\mathbf{f}})}{\partial \xi} + \frac{\partial(\theta\hat{\mathbf{g}})}{\partial \eta} - \frac{\partial(\theta\hat{\mathbf{f}}_\mu)}{\partial \xi} - \frac{\partial(\theta\hat{\mathbf{g}}_\mu)}{\partial \eta} = \frac{\theta\mathbf{s}}{J} \tag{20}$$

where $\hat{\mathbf{w}} = \mathbf{w}/J$, $\hat{\mathbf{f}} = (\xi_x\mathbf{f} + \xi_y\mathbf{g})/J$, $\hat{\mathbf{g}} = (\eta_x\mathbf{f} + \eta_y\mathbf{g})/J$, $\hat{\mathbf{f}}_\mu = (\xi_x\mathbf{f}_\mu + \xi_y\mathbf{g}_\mu)/J$, $\hat{\mathbf{g}}_\mu = (\eta_x\mathbf{f}_\mu + \eta_y\mathbf{g}_\mu)/J$, and J is the Jacobian of the grid transformation. The transformation was employed for the ease of treating curved walls and/or nonuniform meshes. Here, only nonuniform Cartesian meshes are used.

A flux-splitting algorithm similar to Steger and Warming's [23] is used for spatial discretization of the inviscid flux. The inviscid flux is split into positive and negative parts according to the signs of the local eigenvalues of the flux Jacobian. A second-order upwind algorithm applied to the split inviscid fluxes yielded overshoots across the mixing layer and causes nonphysical distribution in the species mass fractions. To suppress the overshoots, a second-order upwind total-variation-diminishing (TVD) scheme [24] is employed; the van Leer limiter satisfying the TVD conditions [24] is implemented in evaluating the derivatives of the split inviscid fluxes. Second-order central differencing is used for the viscous flux and a second-order Runge–Kutta multistage scheme is implemented for time marching. Note that because an explicit time marching is used, the size of the time step is limited by the very small grid size at the center of the channel rather than the chemical source terms.

The numerical scheme was tested against flows with known analytic solutions. Simulations of unsteady shock propagations show excellent agreement with the analytic solutions and excellent shock-capturing capability. Viscous diffusion was also tested by simulating an impulsive motion of a flat plate, and the exact transient solution was recovered. Steady-state solutions for a laminar accelerating and reacting mixing layer were compared with the solutions obtained by Cai et al. [6], and excellent agreement was obtained. The numerical simulations of a two-dimensional nonreacting mixing layer were also compared with a numerical study by Davis and Moore [12]. In our simulations, the freestream velocity ratio is the same as that used in their paper. Forced disturbances are used to excite the mixing layer, and pairing and merging of vortices are triggered by the subharmonic frequencies. The study focuses on the effects of the fundamental frequency with its subharmonics on the vortex dynamics. It was found that the vortex-merging patterns, the number of vortices involved in each merging, and the locations at which vortex merging occurs agree very well with the results obtained by Davis and Moore.

III. Boundary Conditions

There are four boundaries in the computational domain; they are the inlet, exit, and upper and lower walls. Values of the conservative variable w and other physical properties must be known at the boundaries at each time step for the closure of the finite difference equations. For simplicity, inviscid boundary conditions are applied on all boundaries.

A. Inlet Conditions for the Unforced Mixing Layers

At the inlet, the density, streamwise velocity, and mass fractions are specified as hyperbolic-tangent functions and the cross-stream velocity is set to zero. For example, u is specified as follows:

$$u(y) = \bar{U}\left[1 + \lambda \tanh\left(\frac{y}{2\delta_\theta}\right)\right] \tag{21}$$

where $\lambda \equiv (U_1 - U_2)/(U_1 + U_2)$, $\bar{U} \equiv (U_1 + U_2)/2$, and δ_θ is a reference value that is a measure of the mixing-layer thickness at the inlet; δ_θ has a value of 0.000125 m in all cases. The density and mass fractions are specified in the same manner. To reduce reflections of waves at the inlet, the local one-dimensional characteristic equations are solved [25,26] at the inlet for pressure. With this formulation, pressure waves coming from the interior can pass through the inlet plane, and other nonspecified quantities can be adjusted accordingly.

B. Inlet Conditions for the Forced Mixing Layers

Inlet disturbances of ρ, u, and v are prescribed at the inlet to perturb the mixing layers. The flow variables are written as the sum of a mean value and a fluctuating component as

$$(u, v, \rho)(x = 0, y, t) = (\bar{u}, \bar{v}, \bar{\rho})(y) + \epsilon_m Re\{(\hat{u}_m, \hat{v}_m, \hat{\rho}_m)(y)e^{-i\omega_m t}\} \tag{22}$$

In the preceding equation, the first term represents the mean value, which is denoted by $\bar{()}$, and the second term represents the real part of the fluctuating component; $\hat{()}_m$ and ω_m are the eigenfunction and the angular frequency of the unstable mode m, respectively. They are determined from the linear stability analysis (see the Appendix). A small real number ϵ_m is used to adjust the magnitude of the fluctuating component. A superposition of the fundamental frequency and its first subharmonic frequency is imposed. The mean quantities are specified at the inlet and held fixed in time, as in the unforced case. Pressure is determined by solving the local one-dimensional characteristic equations [26], and other properties are determined by the thermodynamics relations.

C. Exit Conditions

For the cases without imposed streamwise pressure gradients, the Mach number at the exit is subsonic; therefore, one condition at the exit plane must be specified to maintain uniqueness and well-posedness. At the exit plane, the average value of pressure across the vertical or radial direction is specified. This allows a nonuniform distribution of pressure at the exit plane. To allow passage of waves at the exit, the 1-D Lagrangian derivatives for ρ_i, ρu, and ρv are set to zero. For the cases with imposed streamwise pressure gradients, the flows achieve supersonic speed at the exit; therefore, extrapolation of variables from the interior is applied at the exit plane.

D. Side-Wall Conditions

For all cases, the side walls are treated as inviscid and impermeable. Slip conditions are applied at the walls, the normal component of velocity is zero at the walls, and the temperature gradient in the normal direction is set to zero. The study is aimed at examining the effects of mixing and reaction. So it is viewed as inefficient to commit resources to the resolution of boundary layers on the side walls.

IV. Computational Results

Mixing layers undergoing transition exhibit early development of large coherent structures. In this paper, our main objective is to study the transitional stage of accelerating and chemically reacting mixing layers. For all the mixing layers considered in this paper, the onset of instability occurs naturally as the flow evolves downstream, and forced disturbances are not required for the instability to sustain. In spite of the self-sustained instability, computations with forced disturbances were also performed.

The computational domain is the straight channel shown in Fig. 1. The length l of the channel is 0.1 m or 800 δ_θ, and the height h is 0.06 m or 480 δ_θ, where $\delta_\theta = 0.000125$ m. The chosen computational domain is actually the physical domain of interest. In the present paper, we are performing numerical simulations on a wall-bounded channel with finite dimensions rather than an infinite domain; 481 and 361 grid points are placed in the streamwise and transverse directions of the channel, respectively. The grid points are nonuniformly distributed in such a way that finer grid points are placed near the inlet and across the centerline of the channel. The grid size in the y direction ranges from 1.13×10^{-5} m ($9.04 \times 10^{-2}\delta_\theta$) at the centerline to 8.22×10^{-4} m (6.58 δ_θ) at the side walls; approximately 100 grid points are placed across the initial mixing layer. The grid size in the x direction ranges from 9.18×10^{-5} m ($7.34 \times 10^{-1}\delta_\theta$) at the inlet to 3.0×10^{-4} m (2.4 δ_θ) at the exit. The

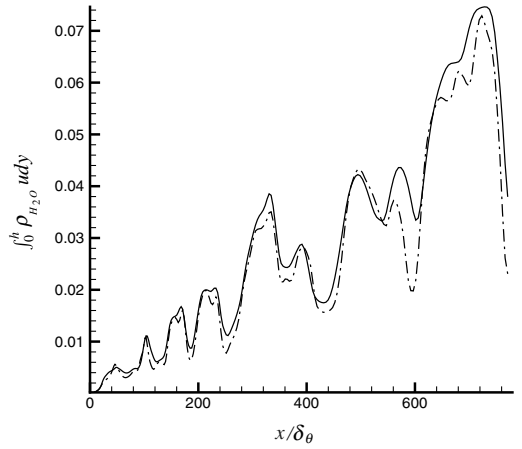

Fig. 2 Instantaneous mass fluxes of H_2O (kg/ms) for the reacting mixing layers versus x locations; 481 × 361 (solid line) and 721 × 541 (dotted–dashed line).

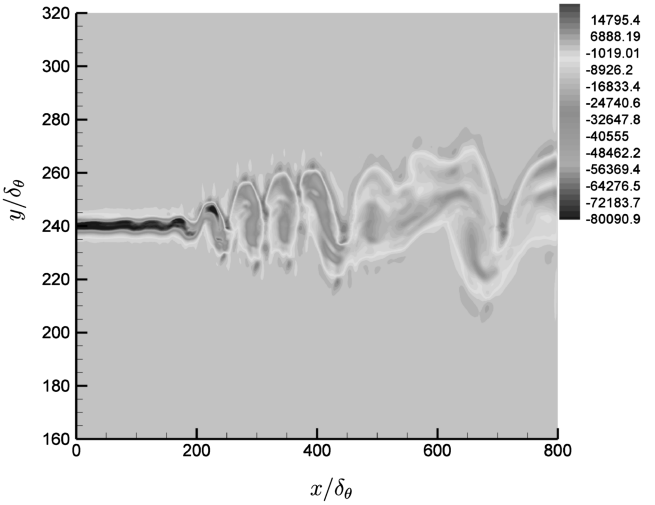

Fig. 3 Instantaneous contours of vorticity (1/s) for the nonreacting and nonaccelerating mixing layer.

481 × 361 grid is comparable with the 721 × 541 grid in resolving the large coherent structures in the reacting mixing layers through the straight channel. The computations for the coarse and fine grids were carried out for approximately 1.2 residence time, so that most of the transient effects were eliminated. The instantaneous mass fluxes of H_2O integrated in the cross-stream direction for the 481 × 361 grid and the 721 × 541 grid at the same instant of time are shown in Fig. 2. In general, good agreement between the two grids is observed, but some smaller structures are resolved better using the finer grid. For other flow variables such as the instantaneous temperature, good agreement is obtained qualitatively, but the quantitative consistency is slightly below of that in Fig. 2. Obtaining grid independence for this transitional reacting flow is quite challenging due to the very fine structures in the mixing region. A paper by Grinstein et al. [27] also observed discrepancies in the development of a shear layer due to grid resolution. From the grid-resolution studies, we confirm that the qualitative behaviors among the four cases are consistent using different grids, and we conclude that some grid dependence remains with the chosen grid (481 × 361), but quantitative accuracy is acceptable and qualitative accuracy is good.

Four cases of mixing layers in a straight channel are studied. The densities of air and fuel are 2.19 and 6.67 kg/m^3, respectively. The initial pressure at the inlet is 10.26 atm. Because the pressure in the channel will be smaller than the inlet pressure, which is below the critical pressure of all species, no supercritical effects need to be considered. Other flow conditions are summarized in Table 1. The streamwise acceleration a_s is calculated by the change in velocity (averaged for the two streams) and the residence time based on the centerline length and the average velocity of the two streams. For all cases, a Courant–Friedrichs–Lewy number of 0.5 is used, and virtually identical results are obtained with smaller Courant–Friedrichs–Lewy numbers. The nonaccelerating mixing layers are discussed in Secs. IV.A and IV.B, and the accelerating mixing layers are discussed in Secs. IV.C and IV.D.

A. Unforced Nonaccelerating Mixing Layers

Numerical simulations of nonaccelerating mixing layers passing through a straight channel were performed. Both the nonreacting and reacting mixing layers become unstable without imposed perturbations. The flow patterns for both the reacting and nonreacting cases are not precisely periodic; that is, the instantaneous vorticity fields appear similar at different times, but the locations of vortex pairings may not be the same at different times.

For the nonreacting mixing layer, the location at which roll-up occurs varies with time. It is observed that the mixing layer starts to roll up between $x = 160\delta_\theta$ to $200\delta_\theta$. The instantaneous contours of vorticity at 3.15 residence time for the nonreacting case are shown in Fig. 3. At this instant of time, the roll-up of the mixing layer starts approximately at $x = 200\delta_\theta$, followed by formation of discrete clockwise vortices further downstream. The larger structure at $x = 700\delta_\theta$ illustrates an amalgamation of two neighboring vortices. Note that this vortex merging occurs occasionally; every pair of neighboring vortices would engage in merging had the subharmonic frequency been imposed.

The same mixing layer but with chemical reactions is now investigated; all the instantaneous results are evaluated at 2.14 residence time. Because of the chemical reactions, the temperature of the reacting mixing layer increases tremendously, and the maximum temperature in the combustion zone is found to be 3260 K. Note that we do not consider dissociation, and so the temperature is higher than practical values. The contours of temperature are shown in Fig. 4. The flame is defined as the location at which a local maximum of temperature in the transverse direction exists. The flame region is indicated in the figure by the darkened area above the dividing streamline, and it is clear that the flame region is biased to the hot-air side. Because of the instability, the ignition region near the inlet oscillates in the x direction, and the amplitude of the waviness of the flame region grows with downstream distance. Multiple peaks in temperature exist across the mixing layer due to the unsteady vortical motions.

We observed that the onset of instability occurs earlier for the mixing layer with chemical reactions; roll-up typically occurs at $x \leq 80\delta_\theta$, and the location varies with time. The instantaneous contours of vorticity are shown in Fig. 5. The roll-up of the mixing layer starts almost immediately downstream of the inlet, at which ignition of the flame occurs. In this ignition region, high volumetric expansion is found due to the heat release. The divergence term $\nabla \cdot u$ attains its maximum value in the ignition region; also, it induces significant cross-stream velocities above and below the ignition

Table 1 Summary of the flow conditions for the straight channel (subscript 1 denotes air and subscript 2 denotes fuel)

	Acceleration	Reaction	u_1, m/s	u_2, m/s	T_1, K	T_2, K	dp/dx, atm/m	$a_s(10^3 g's)$
Case 1	no	no	50	25	1650	300	0	∼0
Case 2	no	yes	50	25	1650	300	0	∼0
Case 3	yes	no	50	25	1650	300	−67	257
Case 4	yes	yes	50	25	1650	300	−67	264

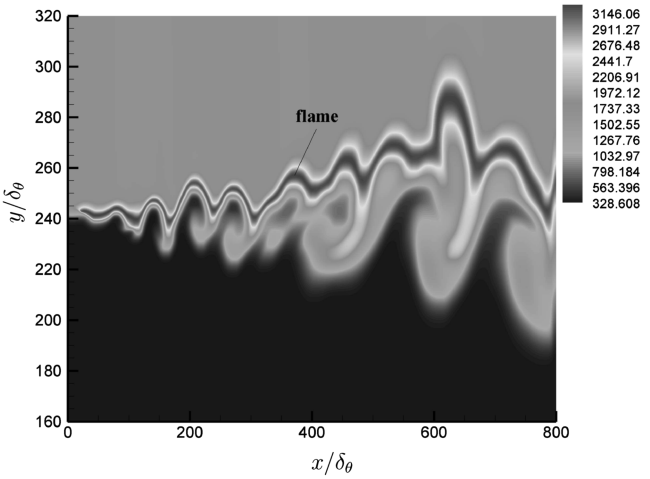

Fig. 4 Instantaneous contours of temperature (K) for the reacting and nonaccelerating mixing layer.

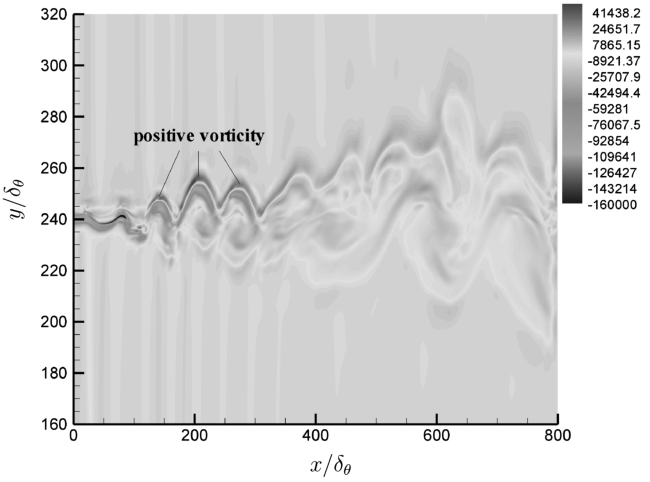

Fig. 5 Instantaneous contours of vorticity (1/s) for the reacting and nonaccelerating mixing layer.

region. Because the flow profiles are significantly altered due to the chemical reactions, it is not surprising that the instability characteristics is different from that for the nonreacting case.

Partly due to the increased viscosity caused by the heat release, the vortices are not as distinct and appear to be more diffusive than those in the nonreacting case. One of the most significant differences between the nonreacting and the reacting cases is the generation of counterclockwise vortices due to the chemical reactions. Regions of positive vorticity are generated in the combustion zone as shown in Fig. 5. The counterclockwise (positive) vortices propagate with the more dominant clockwise (negative) vorticity underneath, and stretching of the vortices causes parts of the negative vortices to break up and engage in merging further downstream. The counter-rotating vortices appear in the combustion regions in which local minimum in density and local maximum in streamwise velocity exist. Although there is no imposed streamwise pressure gradient in the flowfield, a slightly favorable streamwise pressure gradient is generated by the channeled flow itself due to the heat release. This phenomenon can be explained by the classical 1-D flow with heat addition in which streamwise acceleration is achieved without changes in cross-sectional area. Because the lighter fluids in the combustion zone experience relatively higher accelerations, a local maximum in streamwise velocity is produced. The peaks in density and velocity of the time-averaged flowfield are shown in Fig. 6.

To compare the instability between the nonreacting and reacting mixing layers, we define a parameter that measures the ratio of the turbulent kinetic energy to the mean kinetic energy as follows:

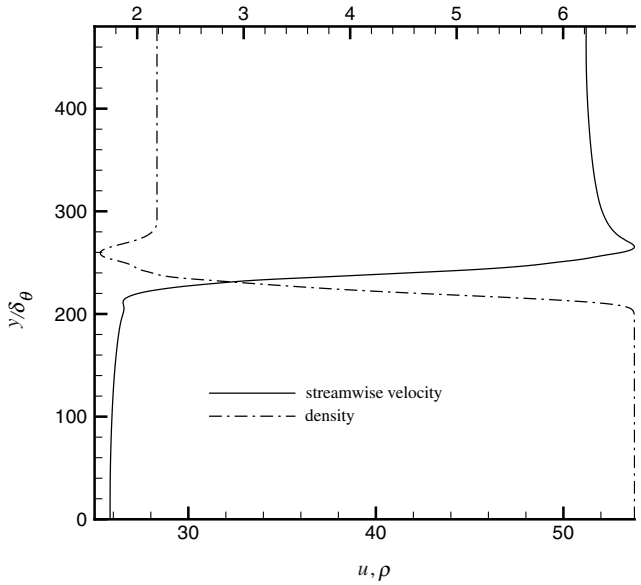

Fig. 6 Time-averaged streamwise and density profiles for the reacting and nonaccelerating mixing layer at $x = 395\delta_\theta$; velocity (m/s) and density (kg/m^3) scales are indicated by the lower and upper x axis, respectively.

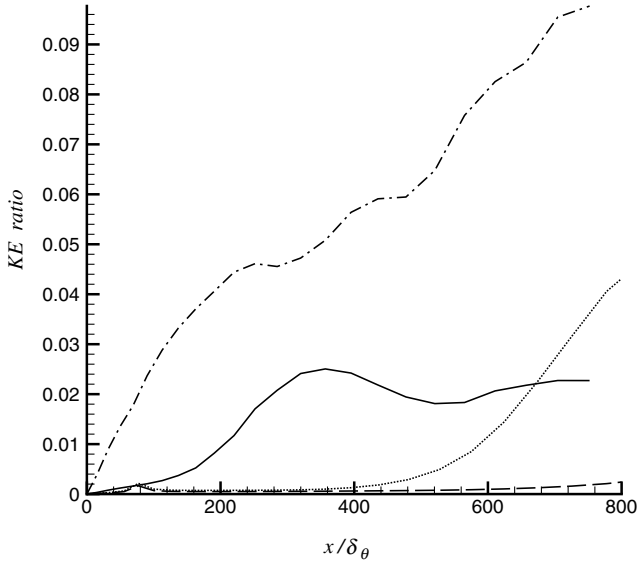

Fig. 7 Ratio of turbulent kinetic energy to mean kinetic energy; case 1 (solid line), case 2 (dotted–dashed line), case 3 (dashed line), and case 4 (dotted line).

$$KE(x) = \frac{\int_0^h \overline{\sqrt{q'^2}}\,\mathrm{d}y}{\int_0^h \bar{q}\,\mathrm{d}y} \tag{23}$$

where $q = \frac{1}{2}\rho(u^2 + v^2)$, $\bar{q}$ is the time average of q, and $q' = q - \bar{q}$. The integral is evaluated at fixed x locations. The results for various cases are shown in Fig. 7. Note that the statistics of the u_{rms}'s also show very similar trends as those in Fig. 7. The statistics for all the cases shown have reached approximately time-independent states; that is, the statistical data are gathered over sufficiently long periods so that further extension of the sampling periods does not cause significant changes in the results. For the nonaccelerating cases, the data are gathered for approximately one residence time, which is 3–4 times as long as the period of the lowest dominant frequency at far downstream locations. Excellent statistically independent results are obtained in the upstream positions. The results are roughly statistically time-independent in the far downstream positions

because of the longer period of the dominant frequency. The results in Fig. 7 indicate that the turbulent kinetic energy is more energetic for the reacting mixing layer, implying that the reacting mixing layer is more unstable than the nonreacting mixing layer. The increased instability also correlates with the larger spreading rate of the mixing region for the reacting mixing layer observed from the vorticity or the temperature contours. The destabilizing effects of the chemical reaction are probably attributed to the modifications of the flow profiles by the chemical reaction; the overshoot in the streamwise velocity and undershoot in the density are of particular importance. The local streamwise velocity peak induces vorticity of both signs; the positive vorticity might impair the vortex-merging mechanism, but the more dominant negative vorticity is also intensified by the increased velocity gradient due to the overshoot. Also, the density gradient has the effect of generating vorticity of both signs through the baroclinic torque.

The finding of the destabilizing effect due to the chemical reaction, however, is different from what other researches [17,19] have found in which the reacting mixing layers showed reduced growth rate compared with the nonreacting mixing layer. The discrepancy might be due to the absence of large gradients of flow properties in the transverse direction in those studies. For the paper by Soteriou and Ghoniem [19], the freestreams of the mixing layers have the same density and temperature, and the normalized enthalpy of reaction is 6. In this paper, however, the initial freestream density ratio (air to fuel) is 0.33, the initial freestream temperature ratio (air to fuel) is 5.5, and the normalized enthalpy of reaction ranges from 2.3 to 7.6 depending on the reference temperature and specific heat being used. Because the density gradient in our study is much larger, the baroclinic effect is more significant, resulting in a more pronounced local velocity peak. Therefore, the instability characteristics could be altered.

B. Forced Nonaccelerating Mixing Layers

In the unforced case, the unstable modes arise naturally due to the development of the mixing layer, and the feedback effects between the inflow and the interior via the propagation of acoustic waves. Therefore, the frequencies of the unstable modes cannot be controlled. In the forced case, the unstable modes are prescribed at the inflow given by Eq. (22), and the effects of the forcing frequencies on the vortex dynamics are investigated.

From the frequency spectrum of the unforced nonreacting mixing layer, the most dominant frequency at positions before any merging of vortices occurs is 4370 hz. This frequency is different from the most unstable frequency (10,504 Hz) predicted by the linear stability theory (LST; see the Appendix) based on the inflow characteristic thickness and flow profiles. In the LST, hyperbolic-tangent profiles are assumed, viscosity is neglected, constant fluid properties in the transverse direction are assumed, and the linear, inviscid calculation is based on the initial thickness at the inlet plane. In the numerical simulation, however, the thickness of the mixing layer increases in the flow direction because of the viscous diffusion and mixing of the species. Therefore, the observed most dominant frequency may not be the same as the one predicted from the linear theory, especially for the reacting case. It is important to point out that the higher frequency predicted by the LST is present in the frequency spectrum of the unforced case, however, it is not the most favorable unstable mode. We chose the forcing frequencies in two different ways:

1) We choose the most unstable frequency ($f_0 = 4370$ Hz) from the unforced nonreacting mixing layer and its first subharmonic frequency ($f_1 = 2185$ Hz) as the forcing frequencies.

2) We choose the most unstable frequency ($f_0 = 10,504$ Hz) from the LST and its first subharmonic frequency ($f_1 = 5252$ Hz) as the forcing frequencies.

Note that the use of a subharmonic frequency is intended to induce vortex merging.

The patterns of the vortices in the forced nonreacting mixing layers appear to be periodic and are more predictable than those in the unforced nonreacting mixing layer. In the unforced case, although vortex merging occurs, the locations of merging and the number of vortices that engage in merging vary with time. In contrast to the unforced case, two vortices always engage in merging at the same x locations in the forced cases. The vorticity contours for the case with forcing frequencies $f_0 = 4370$ Hz and $f_1 = 2185$ Hz are shown in Fig. 8. Two neighboring vortices start the merging at $x \cong 400\delta_\theta$ and complete the merging at $x \cong 520\delta_\theta$; no more merging occurs further downstream. This merging process repeats periodically. For the case with forcing frequencies $f_0 = 10,504$ Hz and $f_1 = 5252$ Hz, vortex merging occurs further upstream, as shown in Fig. 9. Smaller discrete vortices corresponding to the higher fundamental frequency are formed between the inlet and $x \cong 120\delta_\theta$. Every pair of these vortices starts merging at $x \cong 150\delta_\theta$ and completes the merging at $x \cong 200\delta_\theta$. After passing $x = 400\delta_\theta$, the discrete vortices diffuse and merge into a vorticity layer. This vorticity layer rolls up occasionally near the exit. The large structures that appear in the previous forced case are absent here; therefore, the forcing frequencies determined from the LST are not effective in inducing large coherent structures.

For the unforced reacting mixing layer, the most unstable frequency at upstream positions is very close to that in the nonreacting case. Therefore, the same forced disturbances ($f_0 = 4370$ Hz and $f_1 = 2185$ Hz) used in the nonreacting case are applied to the reacting mixing layer. The higher frequencies predicted by LST are not considered because they are less effective in inducing large-scale structures. In the unforced reacting mixing layer, the development of the vortices does not seem to be periodic, and the vortices appear to be more diffusive or smeared. In the forced

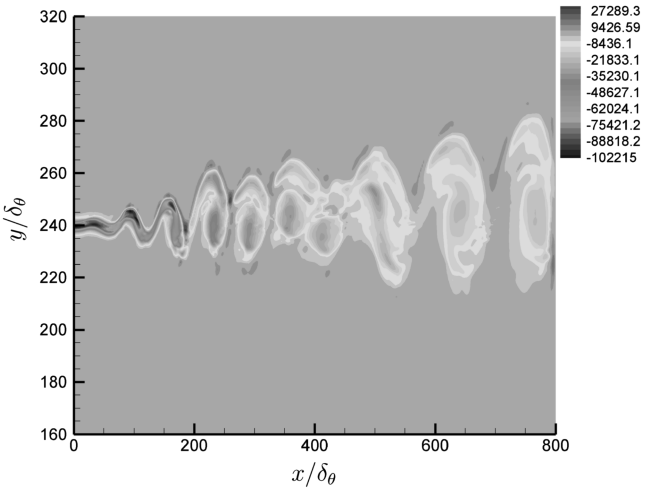

Fig. 8 Instantaneous contours of vorticity (1/s) for the perturbed nonreacting and nonaccelerating mixing layer ($f_0 = 4370$ Hz and $f_1 = 2185$ Hz).

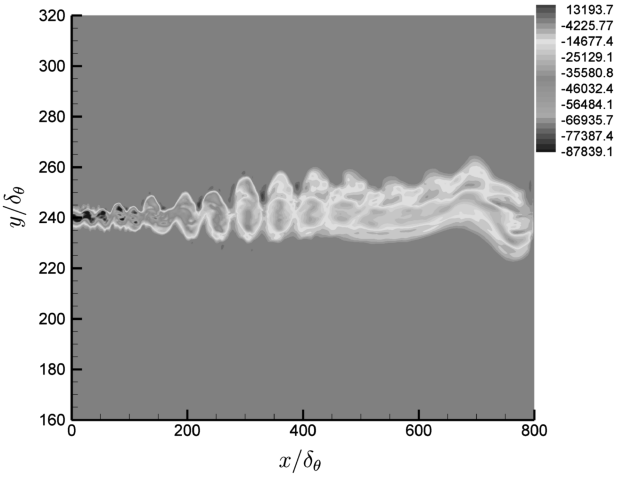

Fig. 9 Instantaneous contours of vorticity (1/s) for the perturbed nonreacting and nonaccelerating mixing layer ($f_0 = 10,504$ Hz and $f_1 = 5252$ Hz).

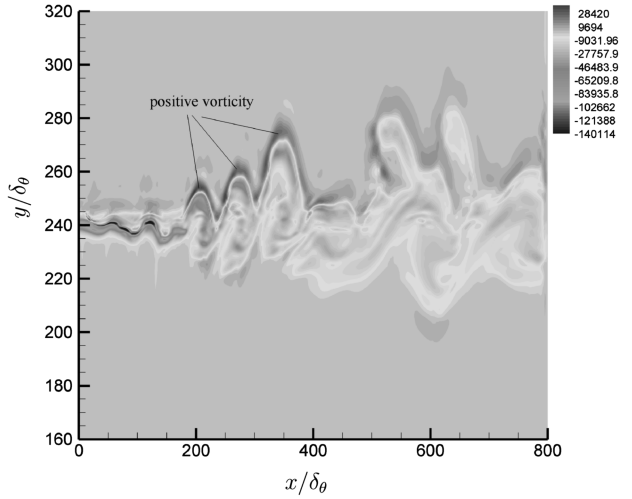

Fig. 10 Instantaneous contours of vorticity (1/s) for the perturbed reacting and nonaccelerating mixing layer ($f_0 = 4370$ Hz and $f_1 = 2185$ Hz).

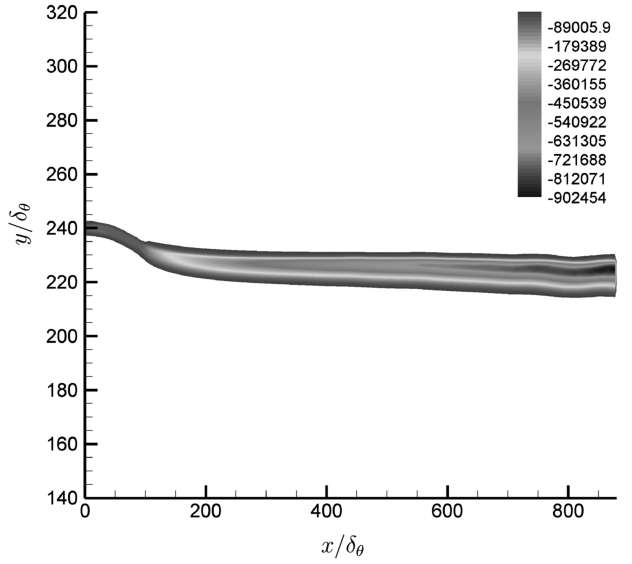

Fig. 11 Instantaneous contours of vorticity (1/s) for the nonreacting and accelerating mixing layer.

reacting mixing layer, the imposed disturbances do not significantly improve the periodicity of the vortices as they do in the corresponding nonreacting cases. Also, the vortex-merging mechanism is similar to that in the unforced case. The positive vortices propagate with the more dominant negative vortices underneath, and parts of the negative vortices break up and engage in merging further downstream. (see Fig. 10).

The preceding results show that the imposed disturbances provide an effective way of manipulating vortex merging in the nonreacting mixing layers, but have little effects on the reacting mixing layer.

C. Unforced Mixing Layers in a Converging–Diverging Channel

Mixing layers with or without chemical reactions under a strong favorable pressure gradient are studied. The inflow conditions are the same as those for the nonaccelerating mixing layers. The instantaneous results for the nonreacting and the reacting cases are presented at times of 2.64 and 2.48 residence time (same residence time for the nonaccelerating case), respectively. Similar to the unforced nonaccelerating cases, the flowfields are also not precisely periodic in time.

The imposed streamwise pressure gradient accelerates the flow tremendously. Because the channel is choked, the mixing layers transit from subsonic speed to supersonic speed through the channel. For the nonreacting mixing layer, the freestream velocities accelerate from a Mach number $\approx$0.06 at the inlet to a Mach number $\approx$1.35 at the exit, and the temperatures and densities drop accordingly. Because the faster airstream is lighter than the fuel stream, the airstream accelerates more than the fuel stream does and hence the difference between the freestream velocities becomes larger with increasing downstream distance. The increasing velocity difference between the freestreams causes the amplitude of the peak vorticity to increase. For this case, the amplitude of the peak vorticity is approximately one order of magnitude as large as that in the nonaccelerating case. Because of the intensified vorticity in the accelerating mixing layer, one expects that the Kelvin–Helmholtz instability is enhanced. On the contrary, it is observed that the streamwise acceleration shows a delay in the development of the unstable structures found in the nonaccelerating cases. The instantaneous contours of vorticity shown in Fig. 11 indicate that the roll-up of the mixing layer is much delayed. The vortex layer does not break into discrete vortices throughout the channel, and the flowfield upstream of the waviness is quite steady in time. Also, the ratio of the turbulent kinetic energy to the mean kinetic energy is much smaller than that in the nonreacting and nonaccelerating case, as shown in Fig. 7. Note that for the accelerating cases, the sampling period of the statistics is about 10 times as long as the period of the lowest dominant frequency far downstream, and statistically independent results are obtained. To investigate the growth of the instability

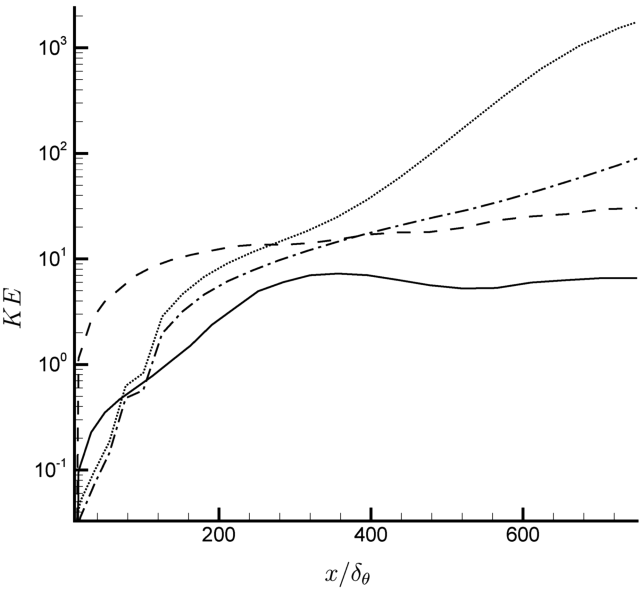

Fig. 12 Turbulent kinetic energy (J/m^2); case 1 (solid line), case 2 (dashed line), case 3 (dotted–dashed line), and case 4 (dotted line).

further, we examine the absolute turbulent kinetic energy rather than its ratio to the mean kinetic energy; that is,

$$KE^*(x) = \int_0^h \overline{\sqrt{q'^2}}\,\mathrm{d}y \tag{24}$$

where q and q' follow the same definitions in Eq. (23). The results for all four cases are shown in Fig. 12. The absolute turbulent kinetic energy for the accelerating and nonreacting mixing layer is, in fact, one order of magnitude larger than that for the corresponding nonaccelerating case. This reveals that the instability for the accelerating case is more energetic than that for the nonaccelerating case in the absolute sense, but the accelerating case is more stable because the growth of the instability is outbalanced by the faster-increasing mean kinetic energy due to the strong acceleration.

Similar to the nonreacting case, the freestreams of the reacting mixing layers accelerate from low subsonic speed at the inlet to low supersonic speed at the exit. However, due to the larger acceleration of the fluids in the low-density combustion zone, a large local maximum in the streamwise velocity is generated. This velocity peak

increases with increasing downstream distance, so that the velocity differences between the peak velocity and the two freestreams become larger. The instantaneous velocity and density profiles across the transverse direction are shown in Fig. 13. Counter-clockwise vorticity is generated above the velocity peak in the combustion zone and clockwise vorticity is generated underneath. Because of the larger velocity gradient below the velocity peak, the clockwise (negative) vorticity is more intense than the counter-clockwise vorticity (positive). The counter-rotating vortices are shown in Fig. 14. The mixing layer is quite steady in the upstream until roll-up of the vorticity layer occurs at $x \approx 550\delta_\theta$. The position of this roll-up appears to be further upstream of that in the corresponding nonreacting case, but further downstream of that in the nonaccelerating and reacting case. By examining the ratio of the turbulent kinetic energy to the mean kinetic energy in Fig. 7, we find that the reacting and accelerating case is more unstable than the nonreacting and accelerating case, but is more stable than the reacting and nonaccelerating case. In terms of the absolute turbulent kinetic energy shown in Fig. 12, the reacting and accelerating mixing layer indeed shows the largest amplitude among all four cases. Similar to the corresponding nonreacting case, the perturbations, however, do not grow as fast as the mean kinetic energy so that the flow is stabilized by the acceleration. Consequently, we conclude that the chemical reactions always destabilize the mixing layers, and the streamwise acceleration always stabilizes the mixing layers. Tearing of the vorticity layer occurs shortly after the roll-up, but merging of like or unlike vortices does not occur within the channel length. Note that although roll-up of the mixing layer occurs in the supersonic regime, we found that the relative velocity of the large structure in mixing zone is always subsonic; therefore, the flows remain shock-free.

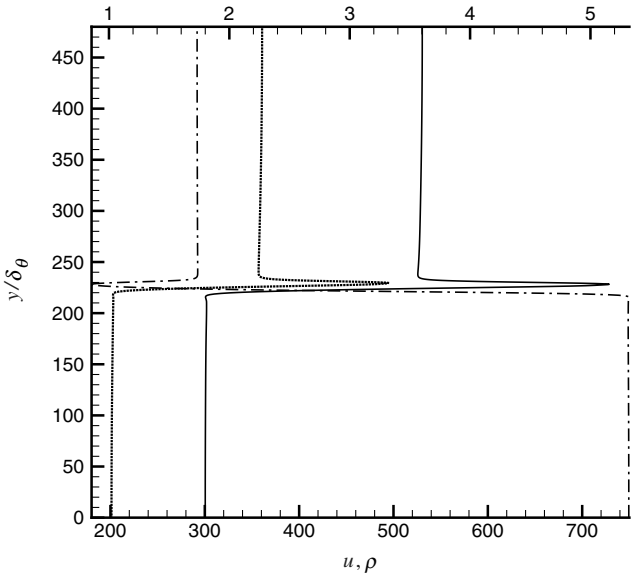

Fig. 13 Instantaneous streamwise velocity and density profiles for the reacting and accelerating mixing layer; streamwise velocity at $x = 400\delta_\theta$ (solid line), streamwise velocity at $x = 240\delta_\theta$ (dotted line), and density at $x = 400\delta_\theta$ (dotted–dashed line); velocity (m/s) and density (kg/m^3) scales are indicated by the lower and upper x axis, respectively.

To gain better understanding of the vorticity dynamics, the dominant terms in the vorticity equation are examined. Because the flow is two-dimensional, the term associated with the deformation of vortex lines vanishes, and the vorticity equation becomes

$$\frac{\mathrm{D}\omega_z}{\mathrm{D}t} = \frac{1}{\rho^2}\nabla\rho \times \nabla p - \omega_z \nabla \cdot \mathbf{u} + \text{viscous term} \qquad (25)$$

We found that the viscous term is, in general, one order of magnitude smaller than the other terms; therefore, we only focus on the production of vorticity associated with the barotropic effects and the divergence of the velocity field. For the accelerating mixing layers with or without chemical reactions, our numerical results indicate that the barotropic term [first term on the right-hand side of Eq. (25)] is comparable in magnitude with the divergence term (second term on the right-hand side of Eq. (25) without the negative sign), and in the laminar region, both terms always have the same sign as the local vorticity, but the barotropic term is always larger in magnitude. In other words, those terms are actually competing against each other; the barotropic effect intensifies the vorticity, but the effect of the expansion weakens the vorticity (indicated by the negative sign in front of the divergence term). Finally, the vorticity increases in magnitude because the barotropic effect is more significant. The instability can be investigated from the perspective of fluctuations in the vorticity production terms. We first define the rms of the barotropic term or the divergence term over time, which is a function of spatial locations. Then the total rms is obtained by integrating the rms in the transverse direction, which results in a function of x locations only. The total rms of the barotropic term and the divergence term for both the nonreacting and reacting cases with acceleration are shown in Fig. 15. In general, the total rms for the reacting case are more than one order of magnitude as large as the

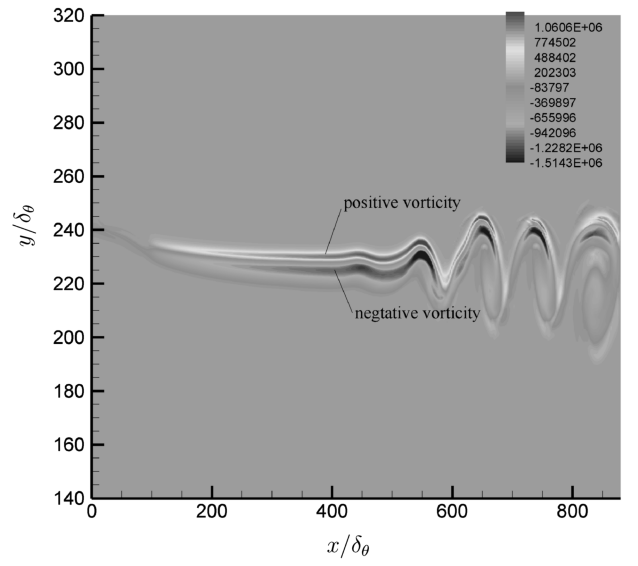

Fig. 14 Instantaneous contours of vorticity (1/s) for the reacting and accelerating mixing layer.

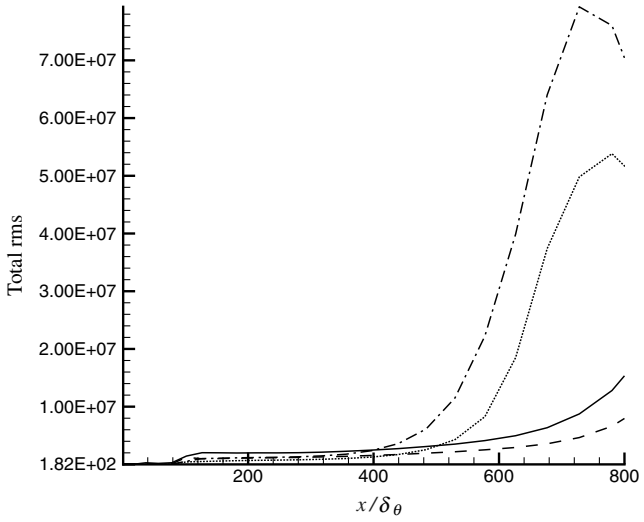

Fig. 15 Total rms (1/s^2) of the barotropic and the divergence terms; case 3 barotropic term (solid line), case 3 divergence term (dashed line), case 4 barotropic term (dotted–dashed line), and case 4 divergence term (dotted line).

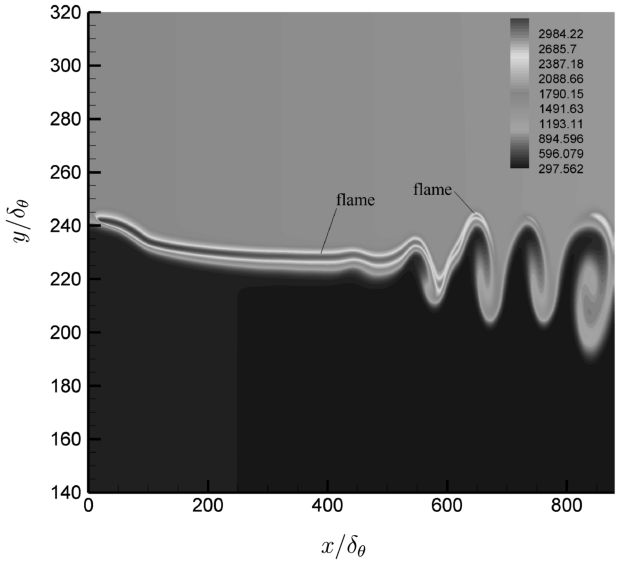

Fig. 16 Instantaneous contours of temperature (K) for the reacting and accelerating mixing layer.

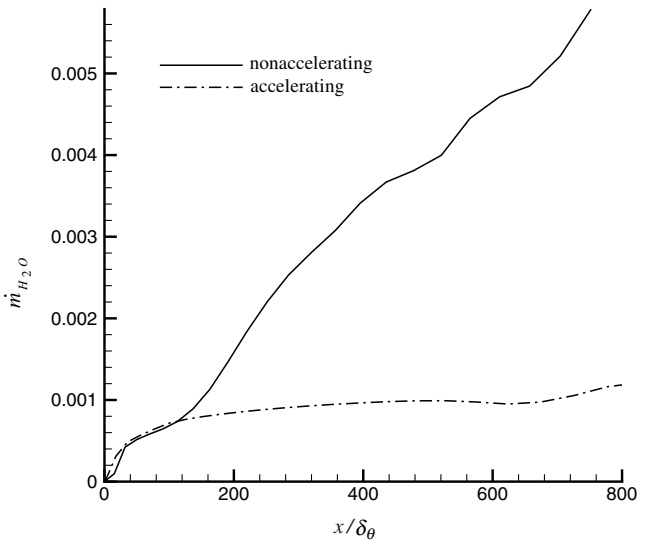

Fig. 17 Formation of H_2O along the channel for the reacting mixing layers.

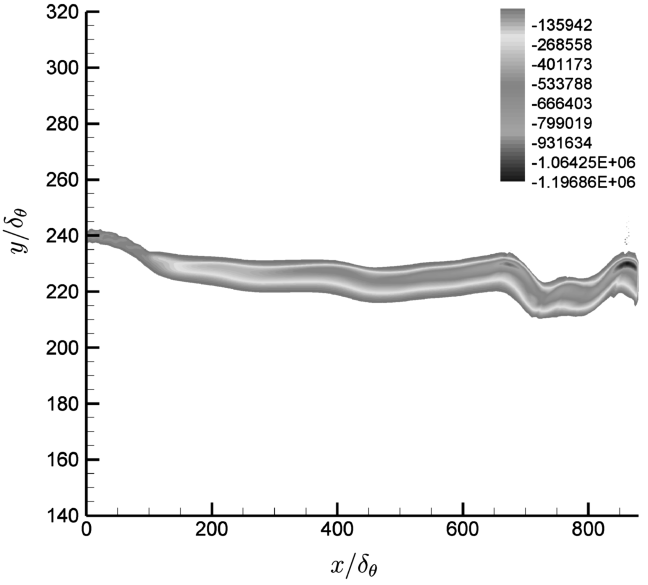

Fig. 18 Instantaneous contours of vorticity (1/s) for the perturbed nonreacting and accelerating mixing layer ($f_0 = 27,150$ Hz and $f_1 = 13,575$ Hz).

total rms for the nonreacting case. This indicates that the reacting case is more unstable than the nonreacting case and is consistent with the finding obtained from the previous analysis of kinetic energy. For both the nonreacting and reacting cases, the total rms of the barotropic term is larger than the total rms of the divergence term.

The chemical reactions and the streamwise pressure gradient cause interesting development of the flame structure not seen in the nonaccelerating case. The instantaneous contours of temperature are shown in Fig. 16. The flame corresponds to the high-temperature region indicated by the thin dark region that curves downward. In general, the peak temperature drops with increasing streamwise distance due to the thermal expansion under acceleration. The peak temperature near the inlet is approximately 3280 K, and the peak temperature at $x \approx 500\delta_\theta$ before roll-up occurs is approximately 2900 K. The flame is smooth initially but waviness develops downstream due to the instability. As the flame propagates downstream, stretching occurs and the flame tears into fragments eventually. We define flame tearing as the condition in which the local peak temperature drops below 2200 K. Because of the tearing, there are regions in which flame extinctions occur and the reaction rates become very low. To investigate the effect of streamwise acceleration on the chemical reaction rate, we compare the average formation of H_2O along the channel. We define the ratio of the mass flow rate of H_2O over the total mass flow rate as follows:

$$\dot{m}_{\mathrm{H_2O}} = \frac{\int_0^h \bar{\rho}_{\mathrm{H_2O}} \bar{u}\, \mathrm{d}y}{\int_0^h \bar{\rho}\, \bar{u}\, \mathrm{d}y} \tag{26}$$

where $\bar{()}$ represents time-averaged quantity, and the integrals are evaluated at fixed x locations. Because the products of H_2O and CO_2 are formed, diffused, and advected in stoichiometric proportions, the mass flux calculation in Eq. (26) indicates the amount of product that was created in the flow up to a specified streamwise position. It can be used as a measure of the efficiency of the chemical conversion process (i.e., mixing plus chemical reaction). Figure 17 shows that the formation of H_2O for the nonaccelerating mixing layer dominates that for the accelerating mixing layer, except in a very small region near the inlet. This implies that the mixing layer without streamwise acceleration is more efficient in combustion. As the flow accelerates through the channel, the mixing due to species diffusion is limited because the residence time is significantly reduced, and hence the chemical conversion rate decreases.

D. Forced Mixing Layers in a Converging–Diverging Channel

In this section, the effects of imposed disturbances on the accelerating mixing layers are investigated. As in the nonaccelerating cases, the forcing frequencies are estimated from the unforced cases. For the accelerating and nonreacting case, the dominant frequency that corresponds to the waviness near the exit is equal to 27,150 Hz; therefore, a fundamental frequency f_0 of 27,150 Hz and its first subharmonic frequency f_1 are chosen as the forcing frequencies. For the accelerating and reacting mixing layer, the roll-up of the vorticity layer begins at approximately 550 δ_θ, and the dominant frequency at that location is equal to 30,170 Hz. With an intention to further excite the roll-up and induce vortex merging, the fundamental frequency f_0 at that location and its first subharmonic frequency f_1 are chosen as the forcing frequencies. Note that the fundamental frequencies of the accelerating flows are several times higher than those in the nonaccelerating flows because the streamwise velocities in the accelerating flows are much higher. For the nonreacting and accelerating mixing layer, the imposed disturbances enhance the development of instability in the mixing layer. The instantaneous contours of vorticity are shown in Fig. 18. It is evident that the waviness of the vorticity layer is more pronounced than that in the unforced case; however, breakup of the vorticity layer as observed in the unforced accelerating and reacting case does not occur. For the reacting and accelerating mixing layer, the effects of

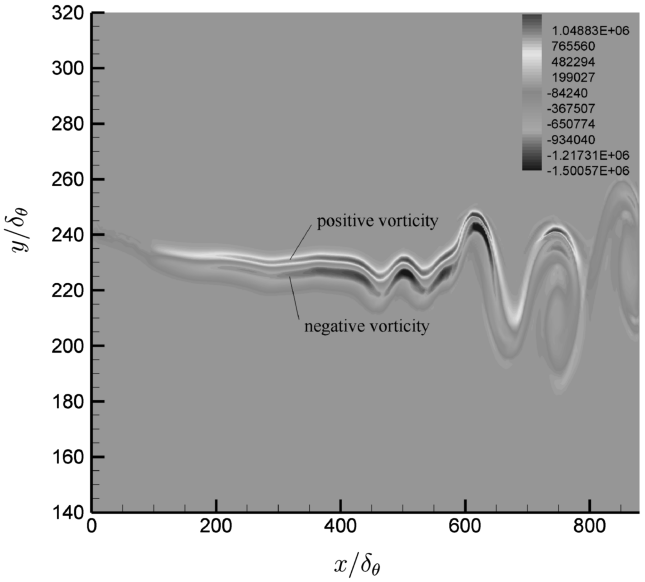

Fig. 19 Instantaneous contours of vorticity (1/s) for the perturbed reacting and accelerating mixing layer ($f_0 = 30,170$ Hz and $f_1 = 15,085$ Hz).

the imposed disturbances are not very obvious. The instantaneous contours of vorticity for this case are shown in Fig. 19. Comparing this with the corresponding unforced case, the upstream portion of the vorticity layer appears more wavy, and the roll-up of the layer is slightly enhanced at $x \approx 500\delta_\theta$. However, the imposed subharmonic frequency does not induce any vortex merging, and the basic flow physics for the forced and unforced cases remain the same. Again, the effects of the imposed disturbances are not significant, and the value of imposing perturbations is limited in our study.

V. Conclusions

Numerical simulations on nonaccelerating and accelerating mixing layers with or without chemical reactions are performed, and the effects of the chemical reactions and the favorable pressure gradient are investigated. For the nonaccelerating and reacting mixing layers, new structures (not found in the corresponding nonreacting case) such as the local peak velocity in the combustion zone and the counter-rotating vorticity are identified. The counter-rotating vortices have also been observed by other researchers [17,19]. One major difference with their findings is that they found that the growth rate of the reacting mixing layer decreased due to the heat release, but we found that the mixing region is thicker and the instability of the reacting mixing layer is more energetic, based on the ratio of the turbulent kinetic energy to the mean kinetic energy. The enhanced instability in our cases is probably caused by the modified flow profiles: that is, the pronounced overshoot in the streamwise velocity and the large density gradients in the transverse direction.

Accelerating mixing layers with or with chemical reactions show stabilizing effects compared with their nonaccelerating counterparts. The onsets of the roll-up of the accelerating mixing layers were much delayed; however, the absolute turbulent kinetic energies are actually orders of magnitude larger than those for the nonaccelerating cases. The stabilizing effect is still possible because the increase in the mean kinetic energy due to the acceleration is more dominant so that the perturbations relative to the mean flow become less significant. In accord with the nonaccelerating cases, the accelerating and reacting mixing layer is also more unstable than the accelerating and nonreacting case. The acceleration along with the chemical reactions cause large overshoots in flow properties across the mixing layer, and this reinforces the conjecture that the modified flow profiles are more susceptible to instability. The streamwise acceleration also causes the global volumetric conversion rate to decrease because of the reduced residence time. Although the some small-scale structures are not resolved due to the resolution of the grid, the instability characteristics is unlikely to be altered because the instability is more related to the mean flow profiles and the large-scale coherent structures, which are well resolved on the current grid. The small-scale structures, however, do affect the combustion process so that the absolute chemical conversion rate may be affected, but the comparisons for the four cases should still be valid.

The effects of forced disturbances were investigated. We found that the forced disturbances do not induce new flow structures or show new physics; therefore, we conclude that the use of forced disturbances is not essential to our research.

Finally, the present numerical simulation could be extended to 3-D. In a 3-D simulation, the spanwise variations of the flowfields will be solved for and the geometry of the converging–diverging channel could be modeled more accurately. The formation and evolution of the streamwise vortical structures in an accelerating and reacting mixing layer would be a very interesting problem for future studies.

Appendix: Linear Stability Theory

The linear stability equations are derived from the compressible Euler equations [28]. The chemical and viscous terms were neglected and uniform properties such as c_p, c_v, and γ are assumed. The flow variables are decomposed into a mean and a small perturbation. Substituting the mean and perturbation quantities into the compressible Euler equations, neglecting the products of small perturbations, and making the assumption of parallel mean flow ($\bar{v} = 0, \partial\bar{u}/\partial x = 0$), one arrives at the following linearized equations:

$$\frac{\partial \rho'}{\partial t} + \bar{\rho}\frac{\partial u'}{\partial x} + \bar{u}\frac{\partial \rho'}{\partial x} + \bar{\rho}\frac{\partial v'}{\partial y} + v'\frac{\partial \bar{\rho}}{\partial y} = 0 \tag{A1}$$

$$\bar{\rho}\frac{\partial u'}{\partial t} + \bar{\rho}\,\bar{u}\frac{\partial u'}{\partial x} + \bar{\rho}v'\frac{\partial \bar{u}}{\partial y} + \frac{\partial p'}{\partial x} = 0 \tag{A2}$$

$$\bar{\rho}\frac{\partial v'}{\partial t} + \bar{\rho}\,\bar{u}\frac{\partial v'}{\partial x} + \frac{\partial p'}{\partial y} = 0 \tag{A3}$$

$$\bar{\rho}\left(\frac{R}{\gamma - 1}\right)\left(\frac{\partial T'}{\partial t} + \bar{u}\frac{\partial T'}{\partial x} + v'\frac{\partial \bar{T}}{\partial y}\right) + \bar{p}\left(\frac{\partial u'}{\partial x} + \frac{\partial v'}{\partial y}\right) = 0 \tag{A4}$$

$$p' = R\bar{\rho}T' + R\rho'\bar{T} \tag{A5}$$

where $\bar{()}$ represents a mean quantity and $()'$ represents a small perturbation. The small perturbations are now modeled by the general form of two-dimensional traveling waves. They are given by

$$(u, v, \rho, p, T)'(x, y, t) = (\hat{u}, \hat{v}, \hat{\rho}, \hat{p}, \hat{T})(y)e^{i(\alpha x - \omega t)} \tag{A6}$$

where α is the wave number, and ω is the angular frequency. In temporal analysis, α is real and ω is complex. In spatial analysis, α is complex and ω is real. In the present study, only spatial analysis is considered. After substituting the traveling wave models into the preceding linearized equations, the system of equations can be reduced to a single first-order ordinary differential equation by the method adopted by Day [28]. This method introduces a composite variable χ, defined as

$$\chi \equiv \frac{i\alpha\hat{p}}{\hat{v}} \tag{A7}$$

Now the final form of the linearized stability equation expressed in terms of χ is written as

$$\frac{\mathrm{d}\chi}{\mathrm{d}y} + \chi\frac{(g\chi + \frac{d\bar{u}}{dy})}{\bar{u} - c} - \alpha^2\bar{\rho}(\bar{u} - c) = 0 \tag{A8}$$

where the complex phase velocity c and the new variable g are defined as

$$c \equiv \frac{\omega}{\alpha} \tag{A9}$$

$$g \equiv \frac{1}{\bar{\rho}} - \frac{(\bar{u}-c)^2}{\gamma \bar{p}} \tag{A10}$$

The boundary conditions are determined from the asymptotic behaviors of the linearized equations; they are

$$\chi(y = \pm\infty) = \mp\alpha\sqrt{\frac{\bar{\rho}}{g}}(\bar{u}-c) \tag{A11}$$

In the spatial analysis, a known value of angular frequency ω is input to the stability equation (A8) and the corresponding eigenvalue α and the eigenfunction χ are being sought. The mean-velocity and density profiles are modeled by the hyperbolic-tangent functions as follows:

$$u(y) = \bar{U}\left[1 + \lambda \tanh\left(\frac{y}{2\delta_\theta}\right)\right] \tag{A12}$$

$$\rho(y) = \bar{\rho}\left[1 + \frac{1-s}{1+s}\tanh\left(\frac{y}{2\delta_\theta}\right)\right] \tag{A13}$$

where $\lambda \equiv (U_1 - U_2)/(U_1 + U_2)$, $\bar{U} \equiv (U_1 + U_2)/2$, $\bar{\rho} \equiv (\rho_1 + \rho_2)/2$, $s \equiv \rho_2/\rho_1$, and δ_θ is a reference thickness. Equation (A8) is integrated numerically by a fourth-order Runge–Kutta scheme. With an initial guess of α, the integration starts from $y = \infty$ and $-\infty$ with the appropriate boundary condition (A11) and ends at $y = 0$. A matching condition $\chi(0^+) = \chi(0^-)$ is enforced at $y = 0$, and a Newton–Raphson iterative method is used to update the value of α. Convergence is obtained when $|\chi(0^+) - \chi(0^-)| \leq 10^{-10}$, and the values of α and χ from the last integration are used to evaluate the eigenfunctions.

References

[1] Sirignano, W. A., and Liu, F., "Performance Increases for Gas-Turbine Engines Through Combustion Inside the Turbine," *Journal of Propulsion and Power*, Vol. 15, No. 1, 1999, pp. 111–118.

[2] Liu, F., and Sirignano, W. A., "Turbojet and Turbofan Engine Performance Increases Through Turbine Burners," *Journal of Propulsion and Power*, Vol. 17, No. 3, 2001, pp. 695–705.

[3] Sirignano, W. A., and Kim, I., "Diffusion Flame in a Two-Dimensional, Accelerating Mixing Layer," *Physics of Fluids*, Vol. 9, No. 9, 1997, pp. 2617–2630.
doi:10.1063/1.869378

[4] Fang, X., Liu, F., and Sirignano, W. A., "Ignition and Flame Studies for an Accelerating Transonic Mixing Layer," *Journal of Propulsion and Power*, Vol. 17, No. 5, 2001, pp. 1058–1066.

[5] Mehring, C., Liu, F., and Sirignano, W. A., "Ignition and Flame Studies for an Accelerating Transonic Turbulent Mixing Layer," AIAA Paper 01-0190, 2001.

[6] Cai, J., Icoz, O., Liu, F., and Sirignano, W. A., "Ignition and Flame Studies for Turbulent Transonic Mixing Layer in a Curved Duct Flow," AIAA Paper 01-0180, 2001.

[7] Ho, C. M., and Huerre, P., "Perturbed Free Shear Layers," *Annual Review of Fluid Mechanics*, Vol. 16, 1984, pp. 365–424.
doi:10.1146/annurev.fl.16.010184.002053

[8] Michalke, A., "Vortex Formation in a Free Boundary Layer According to Stability Theory," *Journal of Fluid Mechanics*, Vol. 22, No. 2, 1965, pp. 371–383.
doi:10.1017/S0022112065000812

[9] Freymuth, P., "On Transition in a Separated Laminar Boundary Layer," *Journal of Fluid Mechanics*, Vol. 25, No. 4, 1966, pp. 683–704.
doi:10.1017/S002211206600034X

[10] Winant, C. D., and Browand, F. K., "Vortex Pairing: The Mechanism of Turbulent Mixing Layer Growth at Moderate Reynolds Number," *Journal of Fluid Mechanics*, Vol. 63, No. 2, 1974, pp. 237–255.
doi:10.1017/S0022112074001121

[11] Ho, C. M., and Huang, L., "Subharmonics and Vortex Merging in Mixing Layers," *Journal of Fluid Mechanics*, Vol. 119, June 1982, pp. 443–473.
doi:10.1017/S0022112082001438

[12] Davis, R. W., and Moore, E. F., "A Numerical Study of Vortex Merging in Mixing Layers," *Physics of Fluids*, Vol. 28, No. 6, 1985, pp. 1626–1635.
doi:10.1063/1.864954

[13] Rogers, M. M., and Moser, R. D., "The Three-Dimensional Evolution of a Plane Mixing Layer: the Kelvin-Helmholtz Rollup," *Journal of Fluid Mechanics*, Vol. 243, Oct. 1992, pp. 183–226.
doi:10.1017/S0022112092002696

[14] Moser, R. D., and Rogers, M. M., "The Three-Dimensional Evolution of a Plane Mixing Layer: Pairing and Transition to Turbulence," *Journal of Fluid Mechanics*, Vol. 247, Feb. 1993, pp. 275–320.
doi:10.1017/S0022112093000473

[15] Shin, D. S., and Ferziger, J. H., "Linear Stability of the Reacting Mixing Layer," *AIAA Journal*, Vol. 29, No. 10, 1991, pp. 1634–1642.

[16] Shin, D. S., and Ferziger, J. H., "Linear Stability of the Compressible Reacting Mixing Layer," *AIAA Journal*, Vol. 31, No. 4, 1993, pp. 677–685.

[17] McMurtry, P. A., Jou, W.-H., Riley, J. J., and Metcalfe, R. W., "Direct Numerical Simulations of a Reacting Mixing Layer with Chemical Heat Release," *AIAA Journal*, Vol. 24, No. 6, 1986, pp. 962–970.

[18] McMurtry, P. A., Riley, J. J., and Metcalfe, R. W., "Effects of Heat Release on the Large-Scale Structure in Turbulent Mixing Layers," *Journal of Fluid Mechanics*, Vol. Feb. 199, 1989, pp. 297–332.
doi:10.1017/S002211208900039X

[19] Soteriou, M. C., and Ghoniem, A. F., "The Vorticity Dynamics of an Exothermic, Spatially Developing, Forced Reacting Shear Layer," *Twenty-Fifth Symposium (International) on Combustion*, The Combustion Inst., Pittsburgh, PA, 1994, pp. 1265–1272.

[20] Hermanson, J. C., and Dimotakis, P. E., "Effects of Heat Release in a Turbulent, Reacting Shear Layer," *Journal of Fluid Mechanics*, Vol. 199, Feb. 1989, pp. 333–375.
doi:10.1017/S0022112089000406

[21] Westbrook, C. K., and Dryer, F. L., "Chemical Kinetic Modeling of Hydrocarbon Combustion," *Progress in Energy and Combustion Science*, Vol. 10, No. 1, 1984, pp. 1–57.
doi:10.1016/0360-1285(84)90118-7

[22] White, F. M., *Viscous Fluid Flow*, 2 ed., McGraw–Hill, New York, 1991.

[23] Steger, J. L., and Warming, R. F., "Flux Vector Splitting of the Inviscid Gasdynamic Equations with Application to Finite-Difference Methods," *Journal of Computational Physics*, Vol. 40, Apr. 1981, pp. 263–293.
doi:10.1016/0021-9991(81)90210-2

[24] Hirsch, C., *Numerical Computation of Internal and External Flows, Vol. 2: Computational Methods for Inviscid and Viscous Flows*, Wiley, New York, 1990.

[25] Poinsot, T. J., and Lele, S. K., "Boundary Conditions for Direct Simulations of Compressible Viscous Flows," *Journal of Computational Physics*, Vol. 101, No. 1, 1992, pp. 104–129.
doi:10.1016/0021-9991(92)90046-2

[26] Grinstein, F. F., "Open Boundary Conditions in the Simulation of Subsonic Turbulent Shear Flows," *Journal of Computational Physics*, Vol. 115, No. 1, 1994, pp. 43–55.
doi:10.1006/jcph.1994.1177

[27] Grinstein, F. F., Oran, E. S., and Boris, J. P., "Pressure Field, Feedback, and Global Instabilities of Subsonic Spatially Developing Mixing Layers," *Physics of Fluids A*, Vol. 3, No. 10, 1991, pp. 2401–2409.
doi:10.1063/1.858178

[28] Day, M. J., "Structure and Stability of Compressible Reacting Mixing Layers," Ph.D. Thesis, Stanford Univ., Stanford, CA, 1999.

T. Jackson
Associate Editor